

DAMAGE PREDICTION FOR CONCRETE-ENCASED STEEL PIERS SUBJECTED TO LATERAL CYCLIC LOADING

Hideki NAITO¹, Mitsuyoshi AKIYAMA² and Motoyuki SUZUKI³

¹ *Research Professor, Dept. of Civil and Environmental Engineering, Tohoku University, Sendai, Japan*

² *Associate Professor, Dept. of Civil and Environmental Engineering, Tohoku University, Sendai, Japan*

³ *Professor, Dept. of Civil and Environmental Engineering, Tohoku University, Sendai, Japan*

Email: naito@civil.tohoku.ac.jp, akiyama@civil.tohoku.ac.jp, suzuki@civil.tohoku.ac.jp

ABSTRACT :

This paper presents an experimental and analytical investigation of the seismic performance of concrete-encased steel piers, which are sometimes known as steel-reinforced concrete (SRC) structures. In particular, a ductility evaluation and a damage prediction method for the seismic design of SRC piers are proposed.

First, load-deformation characteristics and plastic curvature distribution were measured in cyclic loading tests of SRC columns. In these tests, two limit states considering the damage level of SRC columns were shown. In this study, the restorable limit state and the ultimate limit state are defined as the spalling of the cover concrete and the local buckling of the H-shaped steel, respectively.

To evaluate the displacement at the restorable limit state, the plastic curvature distribution at the spalling of the concrete cover was modeled to the rectangle distribution, and its curvature was calculated by buckling analysis of the longitudinal bars confined within the cover concrete and the ties. The displacement at the ultimate limit state was calculated by integrating the curvature distribution based on the local buckling analysis of a steel plate fixed in concrete. Using experimental tests including those of other authors, it was confirmed that the proposed method can appropriately evaluate the displacement at the restorable limit state (the spalling of the cover concrete) and the ultimate limit state (the local buckling of the H-shaped steel) of SRC columns.

KEYWORDS: concrete-encased steel piers, cyclic loading tests, ductility evaluation, damage prediction

1. INTRODUCTION

Severe earthquakes occur frequently in Japan. Hence, important structures such as expressways and railways should be designed for safety against large seismic ground motions. Concrete-encased steel structures, sometimes known as steel-reinforced concrete (SRC), have high strength and ductility because concrete and H-shaped steel are integrated. Recently, in Japan, many SRC piers have been constructed because of their high seismic performance. However, the load capacity, large deformation property and damage process of the SRC piers have not been sufficiently clarified, and studies on the seismic performance of SRC piers are few in number. Therefore, the seismic design of SRC piers has referred to that for RC piers. In such a design, the high strength and ductility of SRC piers is ignored. If the damage to SRC piers as a result of large earthquakes, for example, the cracking and spalling of cover concrete and local buckling of longitudinal bars and H-shaped steel, can be predicted appropriately, seismic design of SRC piers considering the restorative efforts required after large earthquakes can be useful. It is necessary to define the limit states of SRC columns corresponding to damage levels and to propose a ductility evaluation and damage prediction method. In this paper, to propose a seismic design method for SRC piers based on the definition of limit states for damage levels, reversal cyclic loading tests of SRC columns were examined. Moreover, theoretical values using the proposed method were compared with experimental results including those of other authors.

2. REVERSAL CYCLIC LOADING TESTS OF SRC COLUMNS

2.1. Outline of Experimental Tests

Reversal cyclic loading tests of 4 SRC columns and 1 RC column were examined. The details of these specimens are shown in Table 2.1 and Figure 2.1. The shear spans are 1500 mm in all of the RC and SRC

Table 2.1 Specimen details

Specimen number	Shear span (mm)	Sectional size (mm)	H-shaped steel		Longitudinal bars			Ties			Concrete strength (N/mm ²)
			Size (mm) $H_s \times B_s \times t_w \times t_f$	Yield strength (N/mm ²)	Diameter (mm)	Number	Yield strength (N/mm ²)	Diameter (mm)	Spacing (mm)	Yield strength (N/mm ²)	
No.0	1500	650×650	(RC column)	---	19	18	424	13	100	435	20.7
No.1S	1500	500×500	300×200×10×15	376	16	10	442	10	100	457	25.3
No.2S			300×80×10×15	293	25	8	436	10	100	390	24.4
No.3S			300×250×10×15	293	13	8	409	10	100	390	25.2
No.4S			300×250×10×15	293	13	8	409	6	300	317	28.6

columns. Each SRC column and RC column has almost the same load capacity under the flexural and shear loading. While the size in the RC section was 650 mm × 650 mm, the size in the SRC sections could be reduced to 500 mm × 500 mm. In this study, specimen No.1S was established as the standard type of SRC column, and specimen No.2S as a reduced ratio of H-shaped steel, and specimen No.3S as an increased ratio of H-shaped steel, respectively. Additionally, to examine the effect of the amount of ties on the seismic performance of SRC columns, specimen No.4S, with a decreased number and diameter of ties from that of specimen No.3S, was designed. In specimens No.1S to No.4S, H-shaped steel is welded with a steel base plate (size 500 mm × 500 mm and 25 mm in thickness) at the bottom of the concrete footing (890 mm in the height).

In these experimental tests, a horizontal cyclic load was added to the top of the SRC columns without axial loading. The material strength of the H-shaped steel, reinforced bars and concrete are shown in Table 2.1.

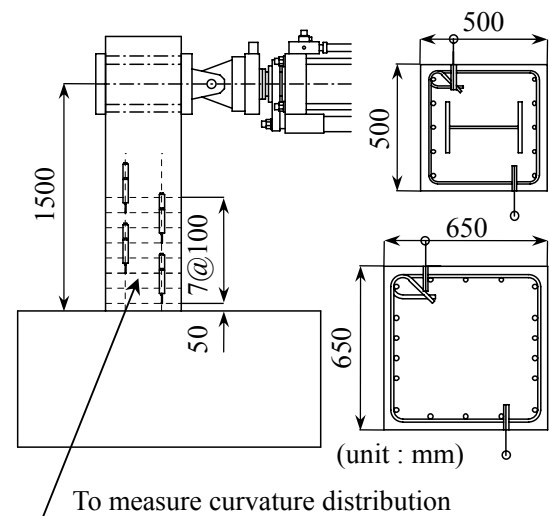


Figure 2.1 Loading arrangements

2.2. Load-displacement Relation and Damage Process

Load-displacement relations from the cyclic loading tests are shown in Figure 2.2. In the experimental results, the damage process of the SRC columns subjected to reversed cyclic loading are shown as the cracking and spalling of the cover concrete, the buckling of the longitudinal bars, the fracture of the longitudinal bars, the spalling of core concrete outside of the H-shaped steel, the local buckling of H-shaped steel (flange plate), and the cracking of the H-shaped steel. The displacement at the spalling of the cover concrete and the local buckling of H-shaped steel are shown in Figure 2.2. Here, these damages are described based on visual observation.

As a comparison of RC and SRC columns, the load-displacement relations of specimens No.0 and No.1S are shown in Figure 2.2. In the experiment on specimen No.0 (RC), the longitudinal bars reached the yield strain at 6.4 mm horizontal displacement, at which point the bending cracks became large and small shear cracks appeared. At 36.2 mm horizontal displacement, the buckling of longitudinal bars caused spalling of the cover concrete; the load-displacement relation shown in Figure 2.2 clearly reflects the decreased load. After the spalling of the cover concrete, the RC columns collapsed because the shear cracks became large.

On the other hand, in specimen No.1S (SRC), the yield displacement is 6.4 mm. At 72.9 mm ($9d_y$) horizontal displacement, even though spalling of cover concrete and buckling of longitudinal bars have occurred, the load capacity does not decrease as in No.0 (RC). In these specimens, the longitudinal bars fracture after buckling. At 143 mm ($15d_y$) horizontal displacement, the core concrete outside the H-shaped steel spalls, and local buckling of the H-shaped steel appears. No.1S appears to have sustained strength and a large energy absorption capacity under cyclic loading at 200 mm horizontal displacement because the H-shaped steel is confined in concrete and cracking in the steel flange does not occur.

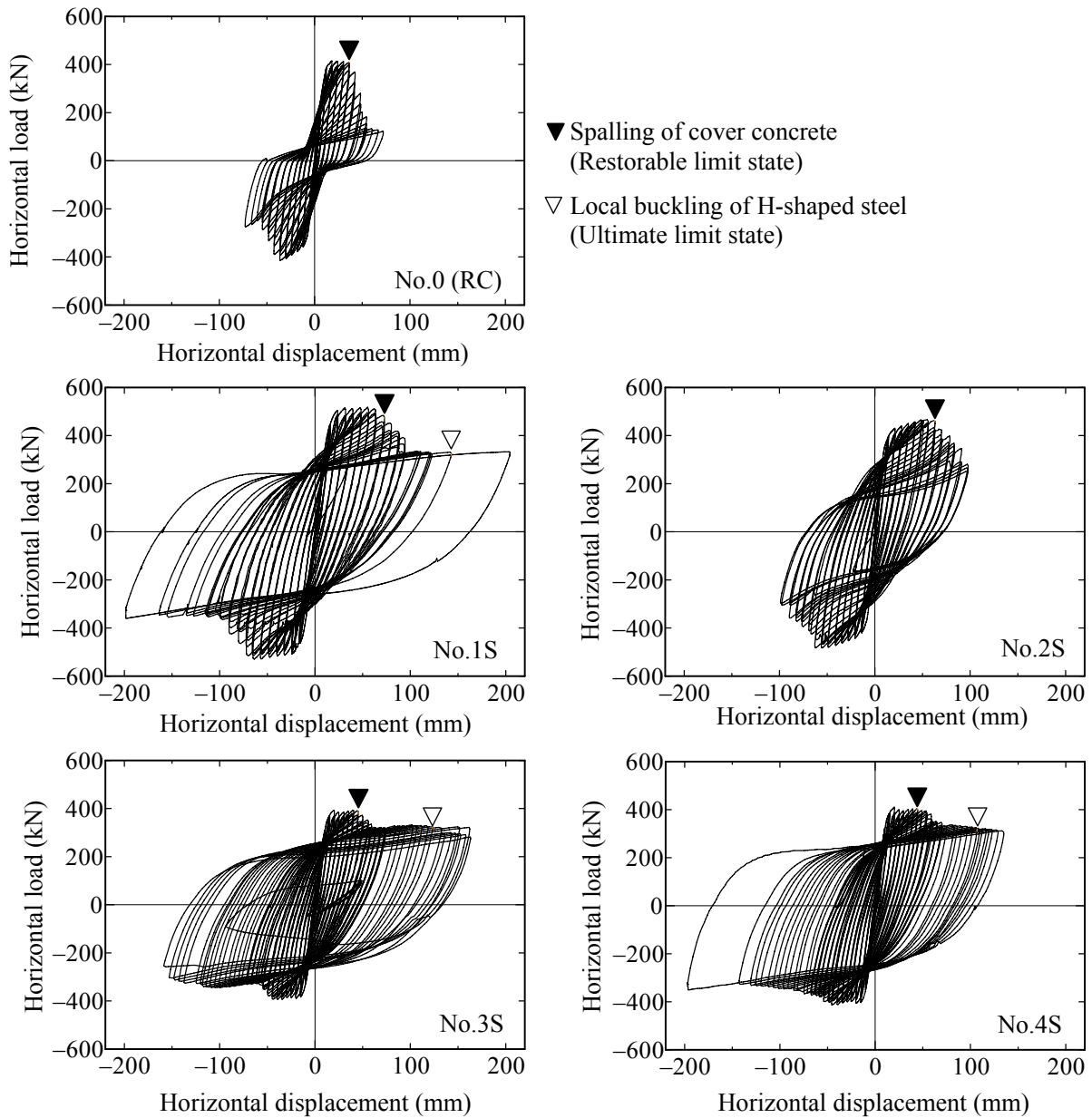


Figure 2.2 Load-displacement relations

Load-displacement relations of No.1S (standard steel content), No.2S (reduced steel content), and No.3S (increased steel content) are compared. In specimen No.2S, with a relatively small steel content, at 55.8 mm ($9d_y$) horizontal displacement, when the spalling of cover concrete and buckling of longitudinal bars occurred, the load decreased and the energy absorption capacity became small. Because the shear cracks were small, the deterioration of the seismic performance of No.2S was caused by the buckling and fracture of the longitudinal bars. Though the concrete outside the H-shaped steel spalled, no local buckling of the flange steel appeared in No.2S. In No.3S with a relatively large amount of steel, both spalling of the cover concrete and buckling of longitudinal bars were induced at 45.3 mm ($9d_y$) horizontal displacement. After the buckling of longitudinal bars, the load capacity and the energy absorption capacity showed little change because of the large steel content. However, at 123 mm ($24d_y$) horizontal displacement, the steel flange buckled in places, with the brittle collapse caused by cracking in the steel flange.

With regard to the amount of ties, No.3S (standard tie content) and No.4S (reduced tie content) were compared. Both these SRC specimens have a large steel content. Despite the different of tie content, the

load-displacement relation and the damage process of No.3S and No.4S were almost same. As No.4S showed no cracking in the H-shaped steel, it demonstrated sustained strength and large energy absorption at 200 mm horizontal displacement.

2.3. Restorable and Ultimate Limit State of SRC Columns

In the seismic design of SRC piers, it is necessary not only to avoid collapse but also to control the damage level for the public importance of the structures. In this study, the ultimate limit state is defined as that required to avoid the collapse of SRC columns, while the restorable limit state is that which can be recovered in the short term without excessive cost.

With regard to experimental tests, for the both RC and SRC columns, enormous damage (e.g., the buckling and fracture of longitudinal bars) is caused after the spalling of the cover concrete. Therefore, the spalling of cover concrete is the common restorable limit state for RC and SRC columns. If the dynamic responses of the SRC members remain within this restorable limit state, the structure can be repaired in the short term by crack injection repair, etc. On the other hand, with regard to the experimental tests, SRC columns with a large steel content have high ductility and large energy absorption after the spalling of the cover concrete. For instance, in rigid-frame piers, excessive displacement in the overall system of the pier is not caused even if some members become plastic. It seems that it is also possible to allow a response greater than the restorable limit state in some plastic hinges and to use the ultimate limit state if the public importance of the structure is low. For such seismic design, it is necessary to define the restorable and ultimate limit state of the SRC piers, and to have a method of evaluating ductility of SRC columns. In these experimental tests, No.3S underwent brittle collapse due to cracking in the steel flange after local buckling. Referring to other experimental reports, SRC columns are collapsed by cracking in the steel flange or flange-web weld after the local buckling of the H-shaped steel. However, the damage mechanism of SRC columns before the cracking in the H-shaped steel is not clear, and there are few experimental data. Considering that i) the crack may be caused almost as soon as the local buckling of the steel flange and ii) predicting the cracking of steel flange confined in concrete is difficult, the ultimate limit state has to be defined as the local buckling of the H-shaped steel. If the dynamic response of all SRC members is kept within this ultimate limit state, SRC piers can avoid failure.

In this study, the restorable limit state and the ultimate state are defined as the spalling of the cover concrete and the local buckling of the H-shaped steel, respectively. For the definition of the restoration limit and the ultimate states, a method for predicting these damage states is presented by the buckling analysis model of longitudinal bars and H-shaped steel.

3. DUCTILITY EVALUATION OF THE RESTORABLE LIMIT STATE

3.1. Damage Prediction of the Buckling of Longitudinal Bars

Concrete piers in Japan are usually subjected to axial loading of about 1.0 N/mm². In the experimental tests, the spalling of the cover concrete was caused by the buckling of longitudinal bars in the RC and SRC columns. Referring to our previous study, a damage prediction method of the spalling of cover concrete based on the buckling model was proposed. Then, the restorable displacement of SRC columns could be calculated using the buckling model shown in Figure 3.1.

The equivalent curvature ϕ_{rbuc} of the restorable limit is written as

$$\phi_{rbuc} = -\frac{1}{\alpha_{rb}d_r} \ln \left[\left(\frac{\sigma_{ry}}{E_r} - b_b \Delta \varepsilon_B \right) \left(\frac{2S_w N_{rbuc}}{\pi D_r} \right)^2 - \gamma \right] + \frac{\Delta \varepsilon_B}{d_r} \quad (3.1)$$

$$\Delta \varepsilon_B = \left[\frac{2(D_r/S_w)}{3N_{rbuc}a_x} \left\{ g(N_{rbuc}) \frac{\sigma_{rm}}{\sigma_{ry}} - 1 \right\} \right]^2 \quad (3.2)$$

$$g(N_{rbuc}) = 1 + \frac{a_x \pi N_{rbuc}}{16(D_r/S_w)N_{ru}} \{ q_c N_{rbuc} S_w + Q_w f(N_{rbuc}) \} \quad (3.3)$$

$$f(N_{rbuc}) = \begin{cases} (N_{rbuc}^2 - 1)/N_{rbuc} & (N_{rbuc} \text{ is odd}) \\ (N_{rbuc}^2 + 2)/N_{rbuc} & (N_{rbuc} \text{ is even}) \end{cases} \quad (3.4)$$

$$q_c = k_{qc} \beta_{qc} d_1 D_r \sigma_c^{2/3} \quad (3.5)$$

$$\beta_{qc} = \begin{cases} 1 - 0.75 \varepsilon_{\max} / \varepsilon_c & (\varepsilon_{\max} \leq \varepsilon_c) \\ 0.25 & (\varepsilon_{\max} \geq \varepsilon_c) \end{cases} \quad (3.6)$$

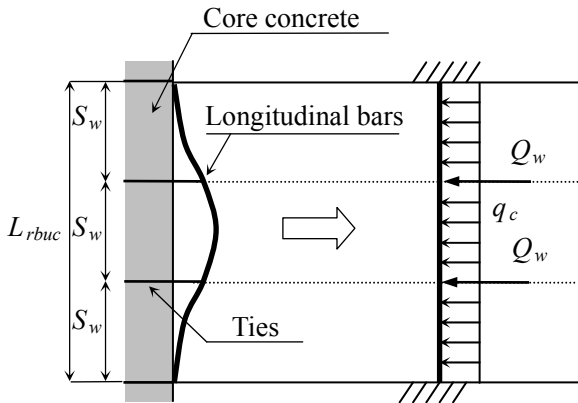


Figure 3.1 Buckling model of longitudinal bars

where $\alpha_{rb}=180$, $\gamma=0.045$, $a_x=0.65$, $b_b=1/100$, $k_{qc}=0.03$, d_r =the distance from the compression bars to the tensile bars in the cross section, N_{rbuc} =the numbers of tie's space in the buckling length L_{rbuc} (for instance, $N_{rbuc}=3$ in Figure 3.1), σ_{ry} =the yield stress of longitudinal bars, E_r =the Young's modulus of the bars, S_w =the spacing of the ties, D_r =the diameter of the bars, σ_{rm} =the tensile strength of the bars, $N_{ru}=A_r \sigma_{rm}$, and A_r =the area of the cross section of the bars. The preservation of the ties is given as $Q_w=a_{we} \sigma_{wy} / N_{rein}$, N_{rein} =the number of the bars on a side of the cross section preserved by the ties, σ_{wy} =the yield strength of the ties, and a_{we} =the effective cross-sectional area of ties given for each tie as $a_{we}=a_w$ (outer tie) and $a_{we}=2.2a_w$ (inner tie) where a_w =the area of the cross

section of a tie itself. And σ_c =the compression strength of the cover concrete, and d_1 =the distance from the center of the cross section of the bar to the edge of the cover concrete. To take the damage by the compression loading into account, the compression strain and the decreased tensile strength are linked by β_{qc} , where ε_c =the compression strain at the maximum strength of the cover concrete, and ε_{\max} =the compression strain of the bar. Here, the numbers of tie's space N_{rbuc} is given as minimum value.

In Figure 3.2, the plastic curvature distribution is modeled to the rectangle distribution with the equivalent curvature ϕ_{rbuc} and the plastic hinge length L_{rP} . Here, the plastic hinge length L_{rP} is written as

$$L_{rP} = L_{p0} \{ (1 + 0.04 t_{ek}) M_m / M_{y0} - 0.25 \} + 12(D_r - 12) \quad (3.7)$$

$$L_{p0} = 0.5d + 0.05h \quad (3.8)$$

where h =the shear span, and d =the effective height of the cross section, t_{ek} =the sectional ratio of the H-shaped steel and longitudinal bars, M_m =the flexural strength (bending moment), and M_{y0} =yield moment.

The restorable displacement δ_{rbuc} is calculated by integration of the rectangle plastic curvature distribution shown in Figure 3.2. It is written as

$$\delta_{rbuc} = \delta_{y0} + (\phi_{rbuc} - \phi_{y0}) (h - L_{rP}/2) h \quad (3.9)$$

where ϕ_{y0} =the yield curvature, and δ_{y0} =the yield displacement.

3.2. Comparison with the Experimental Results

The proposed method was applied and a comparison made between the theoretical values and the 20 experimental values. In the theoretical and experimental values, the effect of the pulling out of the longitudinal bars from the footing is taken into account.

The details of the specimens are as follows: the diameter of bars is 10 mm to 25 mm, the diameter of the ties is 6 mm to 10 mm, the shear span is 1110 mm to 2590 mm, the shear span-to-depth ratio is 3.0 to 7.0, the concrete strength is 23 N/mm² to 32 N/mm², the yield strength of longitudinal and transverse bars is 317 N/mm² to 457 N/mm², the percentage of the volumetric ratio of ties is 0.10 % to 0.79 %, the percentage of the area ratio

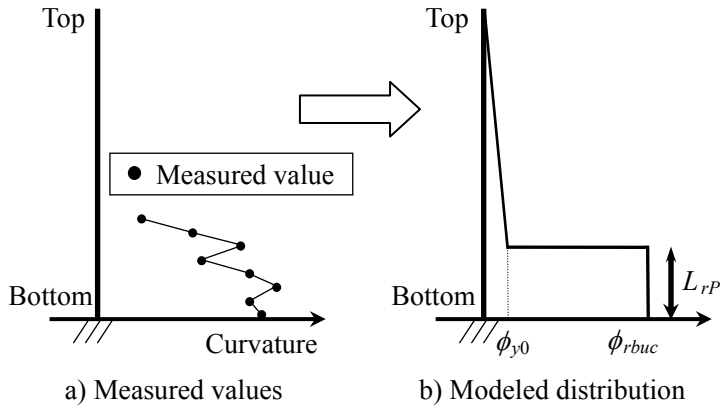


Figure 3.2 Curvature distribution at the restorable state

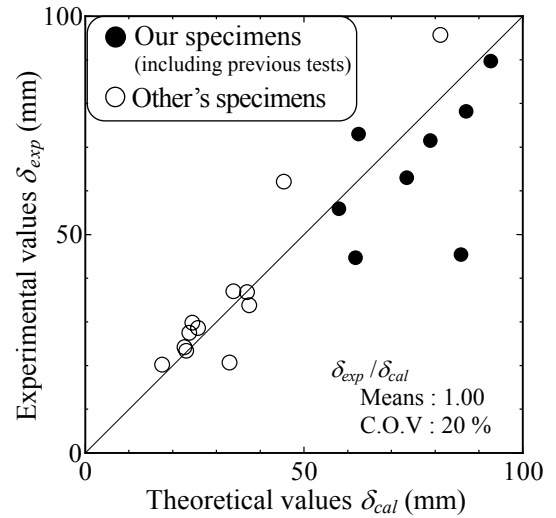


Figure 3.3 Evaluating the restorable displacement

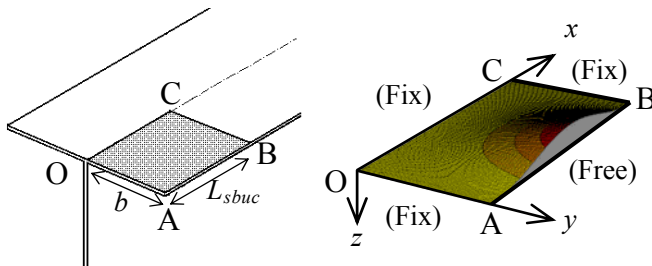


Figure 4.1 Buckling model of steel flange

of the H-shaped steel is 2.53 % to 5.00 %, the percentage of the area ratio of the bars is 0.41 % to 1.62 %, the sectional ratio of the H-shaped steel and longitudinal bars is 1.3 to 10.1, and the axial load is 0 N/mm² to 6.3 N/mm². From the comparison shown in Figure 3.3, it is observed that the results from experimental trials are appropriately evaluated by the proposed method. The mean value and the coefficient of variation of the ratios of the experimental values to the

theoretical values are 1.00 and 20 %, respectively. It is possible to calculate the restorable displacement of SRC columns based on the buckling analysis of longitudinal bars.

4. DUCTILITY EVALUATION OF THE ULTIMATE LIMIT STATE

4.1. Damage Prediction of the Local Buckling of the H-shaped Steel

In reversed cyclic loading tests, SRC columns with a large content of H-shaped steel are known to have high ductility after the spalling of the cover concrete and the buckling of longitudinal bars. However, after the local buckling of the H-shaped steel, SRC columns experience brittle failure by cracking in the steel flange. So, the ultimate limit state is defined as the local buckling of the H-shaped steel.

The ultimate strain (buckling strain) of the steel flange has been formulated considering the concrete fixing. In Figure 4.1, the steel flange is fixed around 3 sides and another side is free. In this study, the deflection of the steel flange w was assumed as

$$w = \delta \sin^2 \frac{\pi x}{L_{sbuc}} \left(1 - \cos \frac{\pi y}{2b} \right) \quad (4.1)$$

where L_{sbuc} =the local buckling length of the steel flange, b =the width of the steel flange, x and y are the axes of the coordinates shown in Figure 4.1. Referring to a previous work, the potential energy within the steel flange is written as

$$\Delta U = \frac{1}{2} D_p \int_0^{L_{sbuc}} \int_0^b \left\{ \kappa_1 \left(\frac{\partial^2 w}{\partial x^2} \right)^2 + 2\kappa_2 \left(\frac{\partial^2 w}{\partial x^2} \right) \left(\frac{\partial^2 w}{\partial y^2} \right) + \kappa_3 \left(\frac{\partial^2 w}{\partial y^2} \right)^2 + 4\kappa_4 \left(\frac{\partial^2 w}{\partial x \partial y} \right)^2 \right\} dx dy \quad (4.2)$$

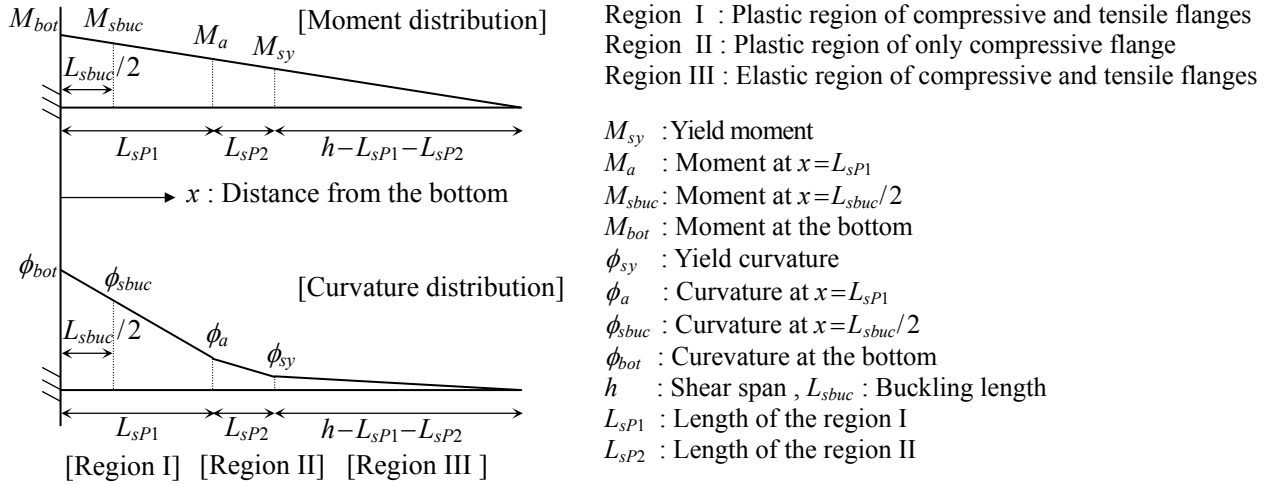


Figure 4.2 Curvature distribution at the ultimate limit state

$$D_p = \frac{E_s t_f^3}{12} \quad (4.3)$$

$$\kappa_1 = \frac{1 + 3(E_{2nd}/E_{sct})}{2 - 4\nu + 3(E_s/E_{sct}) - (1 - 2\nu)^2(E_{2nd}/E_s)} \quad (4.4)$$

$$\kappa_2 = \frac{2 - 2(1 - 2\nu)(E_{2nd}/E_s)}{2 - 4\nu + 3(E_s/E_{sct}) - (1 - 2\nu)^2(E_{2nd}/E_s)} \quad (4.5)$$

$$\kappa_3 = \frac{4}{2 - 4\nu + 3(E_s/E_{sct}) - (1 - 2\nu)^2(E_{2nd}/E_s)} \quad (4.6)$$

$$\kappa_4 = \frac{1}{-1 + 2\nu + 3(E_s/E_{sct})} \quad (4.7)$$

$$E_{sct} = \frac{\sigma_{sy} + E_{2nd}(\varepsilon_{sbuc} - \varepsilon_{sy})}{\varepsilon_{sbuc}} \quad (4.8)$$

where ΔU =the potential energy within the steel flange, E_s =the Young's modulus of the steel, ν =the Poisson ratio, t_f =the thickness of the steel flange, σ_{sy} =the yield stress of the steel, ε_{sy} =the yield strain of the steel, E_{2nd} =the stiffening coefficient after the yield of the steel, and ε_{sbuc} =the ultimate strain for the local buckling of the steel flange.

The energy ΔT caused by axial stress is written as

$$\Delta T = \frac{t_f}{2} \int_0^{L_{sbuc}} \int_0^b \sigma_{sbuc} \frac{\partial^2 w}{\partial x^2} dx dy \quad (4.9)$$

The buckling strength σ_{sbuc} is given from the equilibrium equation as $\Delta U = \Delta T$.

$$\sigma_{sbuc} = \frac{D_p \pi^2}{b^2 t_f} \left\{ \left(3 - \frac{8}{\pi} \right) \left(\frac{b}{L_{sbuc}} \right)^2 \kappa_1 + \frac{3}{256} \left(\frac{L_{sbuc}}{b} \right)^2 \kappa_3 + \left(\frac{1}{8} - \frac{1}{2\pi} \right) \kappa_2 + \frac{1}{4} \kappa_4 \right\} / \left(\frac{3}{4} - \frac{2}{\pi} \right) \quad (4.10)$$

$$\sigma_{sy} + E_{2nd}(\varepsilon_{sbuc} - \varepsilon_{sy}) = \sigma_{sbuc} \quad (4.11)$$

The ultimate strain ε_{sbuc} and the buckling strength σ_{sbuc} are given as minimum values.

The plastic curvature distribution of the H-shaped steel column for the ultimate limit state (local buckling of the H-shaped steel) is shown in Figure 4.2.

Moreover, the ultimate displacement of the SRC column is calculated by integrating the plastic curvature. The ultimate displacement δ_{sbuc} is written as

Table 4.1 Evaluation of the ultimate displacement

		Ultimate displacement δ_{sbuc} (mm)	Buckling length L_{sbuc} (mm)	Plastic region L_{sP} (mm)
No.1S	Proposed method	89	192	321
	Experimental result	143	200	250
No.3S	Proposed method	98	125	345
	Experimental result	123	100	350
No.4S	Proposed method	74	237	308
	Experimental result	106	200	350
No.2 (Azuma et al.)	Proposed method	121	66	1165
	Experimental result	150	---	---

$$\delta_{sbuc} = \{ \phi_{bot} L_{sP1} (3h - L_{sP1}) + \phi_a L_{sP} (3h - L_{sP1} - L_{sP}) + \phi_{sy} (h - L_{sP1}) (2h - L_{sP1} - L_{sP}) \} / 6 \quad (4.12)$$

where these symbols are shown in Figure 4.2.

4.2. Comparison with the Experimental Results

In our experimental tests, local buckling of the H-shaped steel was caused in No.1S, No.3S and No.4S. In addition, referring to experimental trials in other author's study, local buckling of H-shaped steel was also caused and underwent brittle collapse due to cracking in the steel flange after local buckling. A comparison between the proposed method and these 4 experimental results including Azuma's specimen is shown in Table 4.1. The theoretical results of the ultimate displacement are smaller than the experimental results. But the local buckling length L_{sbuc} and plastic length L_{sP} ($=L_{sP1}+L_{sP2}$) are almost the same as that in the experimental results.

5. CONCLUSION

This paper presents an experimental and analytical investigation of the seismic performance of SRC piers. As the result of the reversed cyclic loading tests of SRC columns, two limit states considering the damage level of SRC columns were shown. The restorable limit state and the ultimate state were defined as the spalling of the cover concrete and the local buckling of the H-shaped steel, respectively.

Moreover, ductility evaluation and a damage prediction method for the two limit states are proposed. For the prediction of the restorable limit state, the plastic curvature distribution at the spalling of the cover concrete can be calculated by buckling analysis of the longitudinal bars confined by the cover concrete and ties. For the prediction of the ultimate limit state, the curvature distribution can be calculated by the local buckling analysis of the H-shaped steel in concrete. And the restorable and ultimate displacement can be given by integrating these curvature distributions. Comparing the theoretical values and the experimental trials, it has been confirmed that the proposed method can appropriately evaluate displacement at the restorable limit state (the spalling of the cover concrete) and the ultimate limit state (the local buckling of the H-shaped steel) of SRC columns.

REFERENCES

- Akiyama, M., Naito, H. and Suzuki, M. (2003). Calculation method of ultimate curvature of RC and SRC section based on analytical model for axial reinforcement buckling and its application to ductility evaluation of these columns. *Journals of JSCE* **725: V-58**, 113-129.
- Naito, H., Shirahama, N., Akiyama, M., Takada, M. and Suzuki, M. (2006). Ductility evaluation of SRC columns predicting the local buckling of the h-shaped steel. *Journals of JSCE* **62:E-4**, 698-712.